Ceramics-Silikáty 65 (2), 187-197 (2021)
www.ceramics-silikaty.cz doi: 10.13168/cs.2021.0018

STRUCTURE AND PROPERTIES OF GLASS-CERAMICS FROM BLAST FURNACE SLAG WITH DIFFERENT Al_2O_3/SiO_2 RATIO

ZUHAO LI*, #FENG HE*, **, WENTAO ZHANG*, JUNLIN XIE*, **

*State Key Laboratory of Silicate Materials for Architectures, Wuhan University of Technology, Wuhan, 430070, China
**School of Materials Science and Engineering, Wuhan University of Technology, Wuhan, 430070, China

#E-mail: he-feng2002@163.com

Submitted February 24, 2021; accepted April 10, 2021

Keywords: Glass-ceramics, Blast furnace slag, Al_2O_3/SiO_2, Structure, Sintering

Different Al_2O_3/SiO_2 glass-ceramics were prepared from blast furnace slag by sintering method. The structure and properties of glasses or glass-ceramics were investigated by DSC, XRD, SEM, FTIR, ^{27}Al MAS NMR. The DSC results showed that with the increase of Al_2O_3/SiO_2, the glass transition temperature (T_g) first decreased and then increased, reached the minimum when Al_2O_3/SiO_2 was 0.34. The volume density, bending strength and microhardness of glass-ceramics also showed the same variation rule. Structural analysis showed that when the Al_2O_3/SiO_2 increased from 0.19 to 0.34, Q^2 gradually transformed into Q^1 and Q^3; when the Al_2O_3/SiO_2 continued to increase from 0.34 to 0.39, Q^1 and Q^3 decreased while Q^2 increased. The variation of $[AlO_4]$ and $[AlO_6]$ made the glass network structure the loosest when Al_2O_3/SiO_2 was 0.34. Gehlenite was the main crystalline phase in glass-ceramics, and with the increase of Al_2O_3/SiO_2, the precipitation of gehlenite increased, while the precipitation of diopside and hyalophane decreased.

INTRODUCTION

As a basic industry in China, steel industry produces about 200 billion tons of blast furnace slag (BFS) every year [1, 2] [Jia, 2019 #132; Jia, 2019 #132]. Part of the BFS is directly used in low value-added products such as cement, slag brick and subgrade materials, however, a lot of BFS is dumped, which not only occupies land resources, but also causes serious pollution and waste [3]. In addition to some high titanium BFS, the main composition of BFS is CaO, MgO, Al_2O_3 and SiO_2, with the proportion of these four oxides exceeding 90 wt. %, which is similar to the composition of Ca–Mg––Al–Si glass-ceramics, therefore, BFS is an excellent raw material for glass-ceramics [1, 3].

Glass-ceramics are a kind of polycrystalline solid material containing a large number of microcrystalline and glass phases, which are made by controlling crystallization of specific basic glass [4]. The special structure of glass-ceramics makes it have a variety of excellent properties, such as good insulation performance, high mechanical strength, low dielectric loss, etc. [5], which is a kind of products with high added value materials [4]. The preparation of glass-ceramics with BFS as raw material provides a new way for the recovery and utilization of BFS, which can alleviate the stacking and pollution of BFS and effectively improve the added value of the products.

In the composition of BFS, the content of Al_2O_3 and SiO_2 is more than 40 wt. %, in which SiO_2 acts as the glass network former, Si^{4+} is connected in the shape of silicon-oxygen tetrahedron to form the basic network structure of glass. In the meantime, there are different degree of polymerization and depolymerization with different content of SiO_2 in glass, which is directly related to the heat treatment, microstructure and crystal phase [6]. Al_2O_3 is a network intermediate oxide, Al^{3+} can enter the glass network as $[AlO_4]$, making the structure compact; on the other hand, Al^{3+} can also exist in the glass as $[AlO_6]$, causing the depolymerization of the glass network and making the structure loose [7]. In partial systems, Al^{3+} can also act as the element of partial crystal phases when the content of Al_2O_3 is high [8]. Zhang et al. [9, 10] studied the influence of B_2O_3/Al_2O_3 ratio and Al/Na ratio on BFS glass-ceramics, and indicated that Al_2O_3 improved the thermal stability of glass, meanwhile, the crystallization activation energy and network structure were also affected with the change of Al_2O_3 content. Chen et al. [11] also confirmed that, in the study of glass-ceramics with high calcium system, the crystallization activation energy rose and the main crystal phase changed from akermanite to gehlenite with the increase of Al_2O_3. Cheng et al. [12] showed that the workability and kinetic fragility of glass were linked

with the structure, with the increase of SiO_2/Al_2O_3, the non-bridging oxygen in the glass network decreased, and the structure of the glass network became compact, resulting in the increase of the viscosity of the glass melt, meanwhile, the change of SiO_2/Al_2O_3 ratio were responsible for the increase of fragility. The research of Partyka et al. [13] also showed that the variation of SiO_2/Al_2O_3 ratio directly determined the type and content of crystal phase. Therefore, it is important to investigate the influence of SiO_2/Al_2O_3 on the structure and properties of BFS glass-ceramics.

In this paper, based on 60 wt. % BFS, the effects of different SiO_2/Al_2O_3 on the crystal phases, structure and properties of glass-ceramics were studied. In order to further reveal the influence of the Al_2O_3/SiO_2 on the glass network, Fourier Transform Infrared Spectrometer and Solid State Nuclear Magnetic Resonance Spectrometer were used to deeply investigate the microstructure of glass and glass-ceramics.

EXPERIMENTAL

Raw materials and experimental formula

The BFS used in this experiment was from China Baowu Iron & Steel Group. The chemical composition of BFS was measured by X-ray Fluorescence (XRF, Zetium, PANalytical B. V.), as shown in Table 1. This experiment was based on 60 wt. % BFS and supplemented by pure chemical reagent to prepare glass-ceramics. The high content of alkaline earth metal oxide in BFS leads to the high alkalinity of base glass, which is not conducive to the sintering process due to the fast crystallization [14]. Therefore, the reagents were mainly acid oxides such as SiO_2 and Al_2O_3, and small amounts of oxides such as Na_2O, K_2O, BaO and B_2O_3 were added to adjust the glass melting, clarification, homogenization and sintering process. The oxides were introduced by Na_2CO_3, K_2CO_3, $BaCO_3$ and H_3BO_3 respectively. The formula of parent glass is showed in Table 2. The Al_2O_3/SiO_2 in the base glass are different, which are 0.19 (A1), 0.24 (A2), 0.29 (A3), 0.34 (A4) and 0.39 (A5), respectively.

Preparation of glass-ceramics

Glass-ceramics were prepared using conventional sintering method. The melting temperature of the base glass was 1450 °C, the holding time was 1 h. The melted glass liquid was poured into the clear water to obtain the base glass slag. And the glass slag was ground with planetary grinding ball for 30 min and then passed through a 200 mesh sieve to obtain the parent glass powder which was subsequently pressed into 4 × 40 mm strip samples under a pressure of 50 MPa, and then the samples were sintered in a resistance furnace, the sintering temperature was determined by thermal analysis, the heating rate was 10 ºC·min^{-1}, the holding time was 1.5 h.

Characterizations

Thermal analysis of base glass powder was performed using Differential Scanning Calorimetry (DSC, STA449F3, NETZSCH), the temperature range was 0 °C to 1000 °C in the air and the heating rate was 10 °C min^{-1}. The crystal phase was measured by X-ray Diffractometer (XRD, D8 Advance, BRUKER AXS), the scanning range was 10 °C to 70 °C. The micromorphology and element composition of the glass-ceramics was observed by Field Emission Scanning Electron Microscope (FESEM, Zeiss Ultra Plus, Zeiss Germany) with Energy Dispersive Spectrometer (EDS; X-Max 50), the polished surface was etched with HF solution (4 %) for 40 s. The microstructure of both glass and glass-ceramics was measured by Fourier Transform Infrared Spectrometer (FTIR, Nexus, Thermo Nicolet) at range of 400 cm^{-1} to 1400 cm^{-1}. The ^{27}Al NMR spectra of the base glass were measured by Solid State Nuclear Magnetic Resonance Spectrometer (NMR, AVANCE III).

The bending strength (M, MPa) of glass-ceramics was measured by three-point test method, and the calculation formula was as follows:

$$M = \frac{3FL}{2bh^2} \quad (1)$$

where F is the fracture load (N), L is the span (mm), b is the fracture width (mm), and h is the fracture thickness (mm). The bulk density of glass-ceramics was measured

Table 1. Oxide composition BFS (wt. %).

	Al_2O_3	SiO_2	CaO	MgO	BaO	Na_2O	K_2O	SO_3	Fe_2O_3	TiO_2	Others
BFS	15.12	31.92	39.81	8.54	0.12	0.39	0.58	2.16	0.34	0.64	0.38

Table 2. Oxide composition of parent glass (wt. %).

	Al_2O_3	SiO_2	CaO	MgO	BaO	Na_2O	K_2O	B_2O_3	others	Al_2O_3/SiO_2
A1	9.07	48.19	23.89	5.12	3.00	3.00	3.00	2.00	2.73	0.19
A2	11.08	46.18	23.89	5.12	3.00	3.00	3.00	2.00	2.73	0.24
A3	12.87	44.39	23.89	5.12	3.00	3.00	3.00	2.00	2.73	0.29
A4	14.53	42.73	23.89	5.12	3.00	3.00	3.00	2.00	2.73	0.34
A5	16.07	41.19	23.89	5.12	3.00	3.00	3.00	2.00	2.73	0.39

by Archimedes-drainage method. The indentation method was used to measure the Vickers hardness of the glass-ceramics, the loading force was 0.98 N, the loading time was 10 s.

RESULTS AND DISCUSSION

DSC analysis

Figure 1 showed the DSC graph of parent glasses with different Al_2O_3/SiO_2 at heating rate of 10 °C min^{-1}. Table 3 showed the specific characteristic temperature values for A1 to A5, where T_g was the glass transition temperature, T_{c1} was the first crystallization temperature, and T_{c2} was the second crystallization temperature. In Figure 1, there were two obvious exothermic peaks within the range of 780 °C to 900 °C, among which the first crystal peak shape of A1 parent glass was relatively flat.

The DSC curve of the base glass showed that the peak of T_{c1} became sharp and moved towards low temperature gradually for A1 to A5, while T_{c2} showed a trend of moving towards high temperature for A2 to A5. While the charge of Al^{3+} is less than that of Si^{4+}, and the self-diffusion coefficient of Al^{3+} is higher than that of Si^{4+} [15]. Therefore, the higher Al_2O_3 content in the glass was more conducive to atomic diffusion in the crystallization process [15]; then the crystal phase was precipitated on the surface of the glass particle, which increased the viscosity of the glass, hindered the further diffusion of the atomic [16]. The first crystallization peak of the A1 glass was not obvious and the T_{c2} was high, which may be related to the high SiO_2 content, as Si^{4+} can gather the network, increase the viscosity of the glass, hinder the diffusion of atomic inside the glass [17, 18]. Figure 1 and Table 3 showed that T_g decreased first (reached the minimum in A4) and then increased. In this experiment, according to the DSC curve, in order to ensure that the crystallization process of each sample was fully carried out, the sintering temperature of the sample was set at 890 °C and the holding time was 1.5 h.

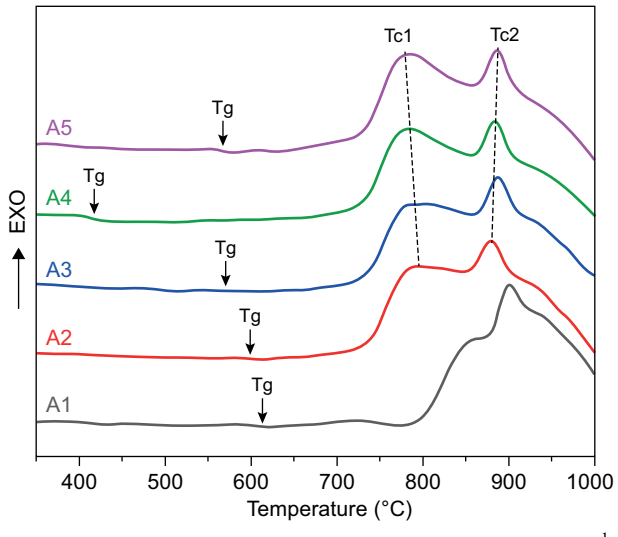

Figure 1. DSC of glasses with different Al_2O_3/SiO_2 at 10 °C min^{-1}.

Table 3. Characteristic temperature (°C) of glasses with different Al_2O_3/SiO_2 in DSC.

	T_g	T_{c1}	T_{c2}
A1	613.7	851.8	900.8
A2	594.7	799.0	880.8
A3	568.8	790.8	886.1
A4	413.1	783.7	886.2
A5	565.2	783.5	887.3

Crystal phase analysis

The XRD graph of glass-ceramics with different Al_2O_3/SiO_2 was illustrated in Figure 2. It showed that the peaks of glass-ceramics were basically the same. The analysis by Jade 6.5 indicated that the crystal phase of glass-ceramics was composed of the main crystal phase gehlenite $(Ca_{1.96}Na_{.05})(Mg_{.24}Al_{.64}Fe_{.12})(Si_{1.39}Al_{.61}O_7)$, PDF#72-2128), the secondary crystal phase diopside($CaMgSi_2O_6$, PDF#74-1607) and hyalophane ($K_{.6}Ba_{.4}Al_{1.42}Si_{2.58}O_8$, PDF#70-0523). Figure 2 also showed that the diffraction peak intensity of the main crystal phase increased while that of the secondary crystal phase decreased gradually for A1 to A5. It means that the content of gehlenite in the glass-ceramics increased while diopside and hyalophane decreased with the increase of Al_2O_3/SiO_2.

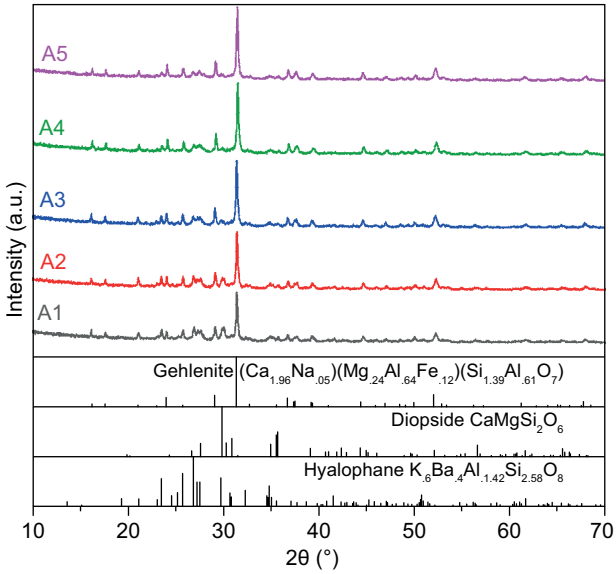

Figure 2. XRD of glass-ceramics with different Al_2O_3/SiO_2.

The Si(Al)/O ratio of anion group $[Si_{1.39}Al_{.61}O_7]$ is smaller than that of $[Si_2O_6]$ and $[Al_{1.42}Si_{2.58}O_8]$, indicating a lower degree of polymerization of $[Si_{1.39}Al_{.61}O_7]$ [19, 20]. In terms of element composition, Al^{3+} directly

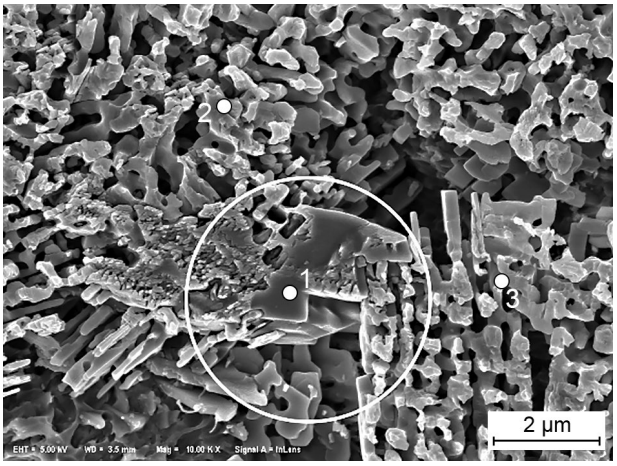

a) A1

participated in the formation of the main crystal phase gehlenite, therefore, the increase of Al_2O_3 content was conducive to the precipitation of gehlenite. On the one hand, with the increase of Al_2O_3/SiO_2, Si^{4+} in the glass decreased and Al^{3+} increased, $[AlO_6]$ played a role in breaking the glass network, reducing the degree of polymerization of glass network and facilitating the precipitation of gehlenite with low degree of anionic polymerization; on the other hand, the increase of Al_2O_3 rose the number of Al^{3+} substituted for Si^{4+} in the glass network, which was conducive to the formation of $[Si_{1.39}Al_{.61}O_7]$ and promoted the precipitation of gehlenite. On account of the large amount of precipitation of gehlenite, Si^{4+} content in the glasses was decreased,

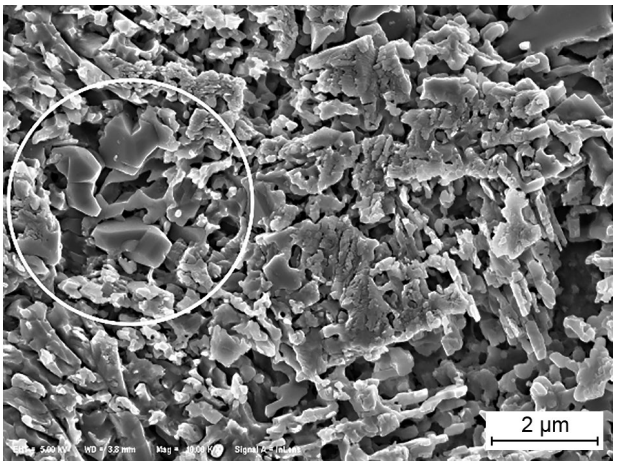

b) A2

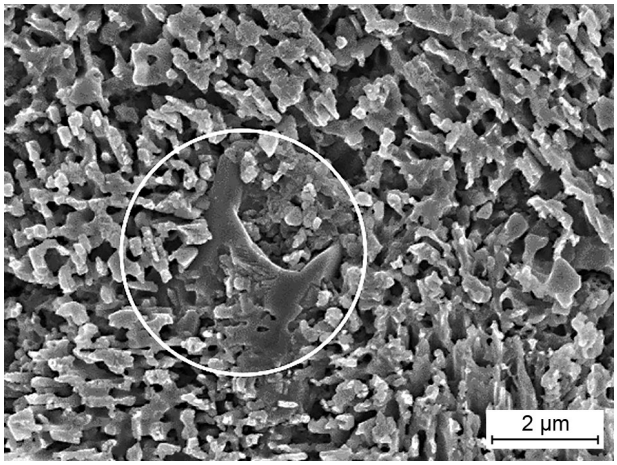

d) A4

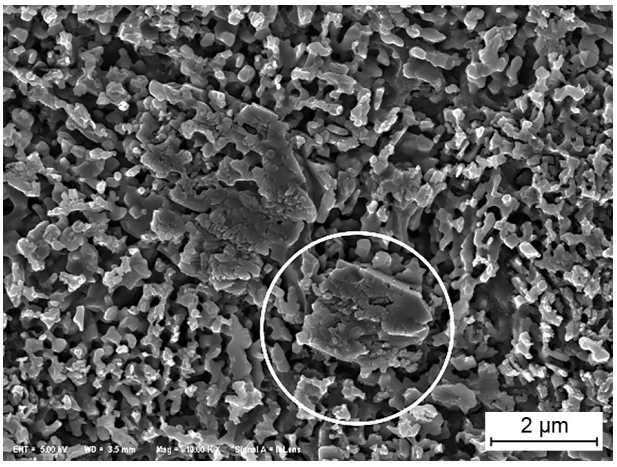

c) A3

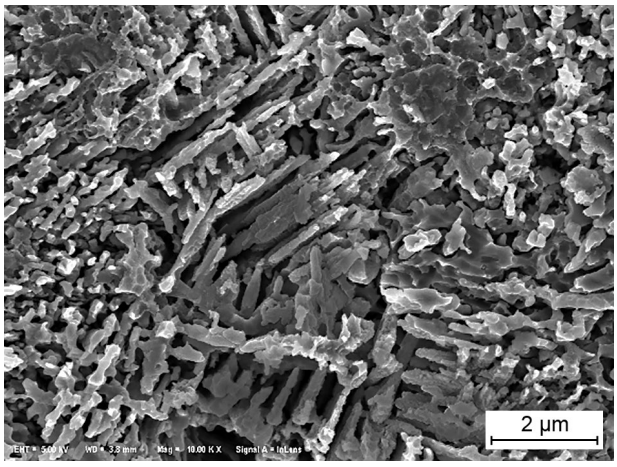

e) A5

Figure 3. SEM of glass-ceramics with different Al_2O_3/SiO_2.

Table 4. Chemical composition (wt. %) of crystals in glass-ceramics.

Point	C	O	Na	Mg	Al	Si	K	Ca	Ti	Fe	Ba
1	10.28	51.73	1.28	1.03	5.69	15.06	2.28	8.50	0.22	0.10	3.83
2	10.52	46.41	1.25	2.89	5.75	16.83	2.37	9.83	0.53	0.22	3.40
3	10.93	44.52	1.64	2.16	5.89	17.32	2.66	10.55	0.27	0.22	3.83

which led to the reduction of the anion group of the secondary crystal phase and reduced the precipitation of diopside and hyalophane.

The SEM morphology graph was showed in Figure 3. It can be seen that the glass-ceramics crystallized fully after sintering, and a large number of isomeric grains were precipitated, meanwhile a small amount of blocky crystal grown in it. In order to further determine the chemical composition of the crystals, FESEM-EDS was used to measure the elemental composition of the grains of A1 glass-ceramics, and the results were listed in Table 4. The content of Mg in point 1 was obviously low. Combining with the XRD results, it was considered that the crystal here was hyalophane. There was no massive grain in A5, which may be related to the small content. Meanwhile, it can be seen that the aspect ratio of grain increased significantly and the grain grown into long strips in A5 glass-ceramics.

FTIR analysis

Figure 4 was the FTIR spectra of the parent glass with different Al_2O_3/SiO_2 at 400-1400 cm^{-1}. There were mainly three wide vibration absorption bands, which were in the range of 400 to 600 cm^{-1}, 600 to 800 cm^{-1} and 800 to 1200 cm^{-1} respectively. The irregular arrangement of ions (ion clusters) in the glass and the existence of non-bridging oxygen bonds made the angle and length of Si–O bond change, which made the infrared vibration absorption peak shift to a certain extent and become gentle and broad [21, 22].

In the infrared vibration spectra of glass, the vibration absorption band in the range of 400 to 600 cm^{-1} was attributed to the bending vibration of Si–O–Si, Si–O–Al, O–Si–O and O–Al–O [23, 24].

The absorption peak in the range of 600 to 800 cm^{-1} was the symmetric stretching vibration of Si–O–Al, which was mainly attributed to the stretching vibration of the $[AlO_4]$ and stretching vibration of the bridge oxygen bond in the glass network structure [11]. From A1 to A5, the vibration absorption peak near 720 cm^{-1} showed a small shift towards low wavenumbers, and the absorption intensity was enhanced, indicating that the Si–O–Al bond with lower vibration frequency in the glass network increased [23]. This was due to the fact that with the increase of Al_2O_3/SiO_2, more and more Al^{3+} entered into the glass network, forming Si–O–Al bond.

The absorption vibration peak in the range of 800 cm^{-1} to 1200 cm^{-1} was mainly related to the $[SiO_4]$, which was attributed to the asymmetric stretching vibration of Si–O–Si, the symmetric stretching vibration and asymmetric stretching vibration of O–Si–O, the absorption was strong and broad, which was caused by the superposition of different peaks [25-27]. The vibration absorption peak in the range of 800 to 1200 cm^{-1} can be

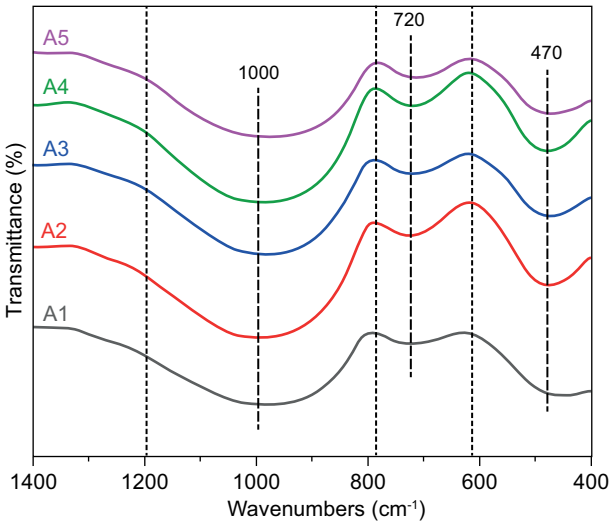

Figure 4. FTIR of glass with different Al_2O_3/SiO_2.

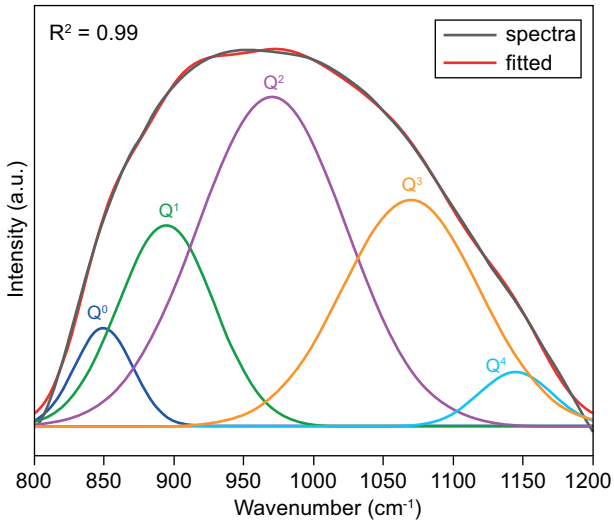

a) A1

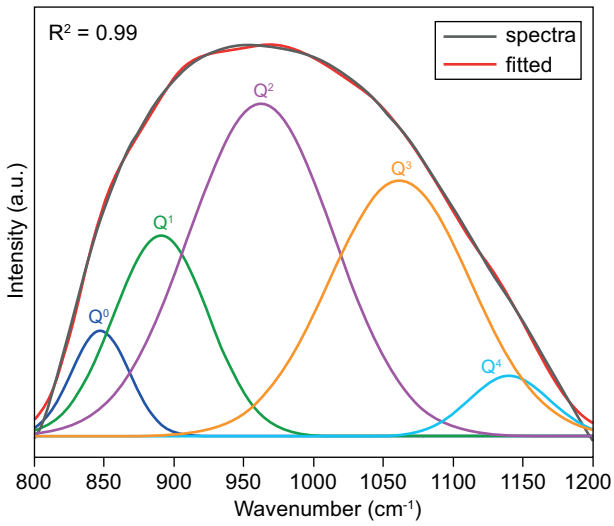

b) A2

Figure 5. Deconvoluted infrared spectra (800 to 1200 cm^{-1}) of glass with different Al_2O_3/SiO_2. *(Continue on next page)*

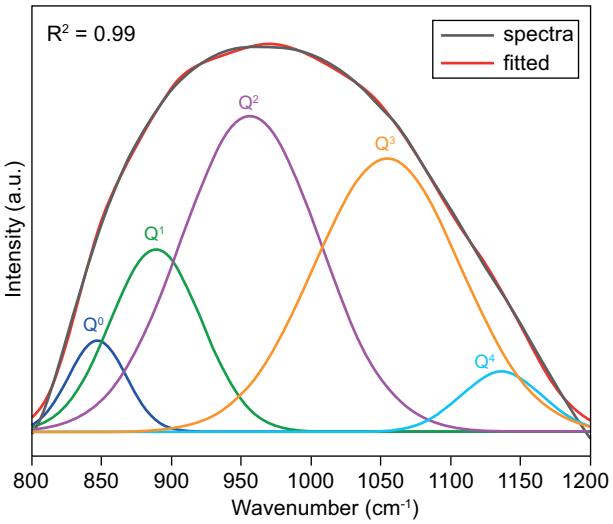

c) A3

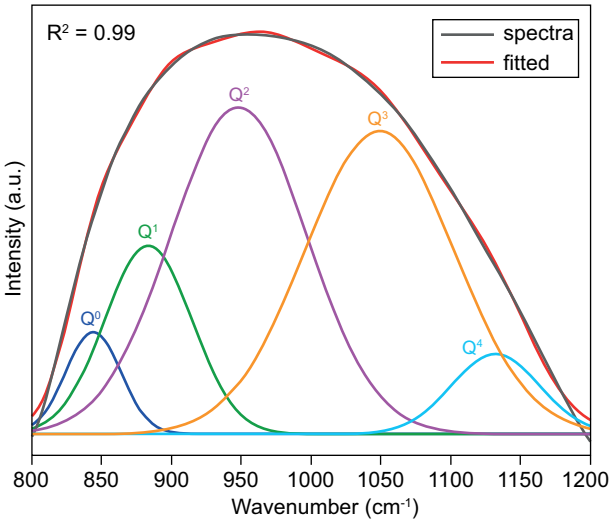

d) A4

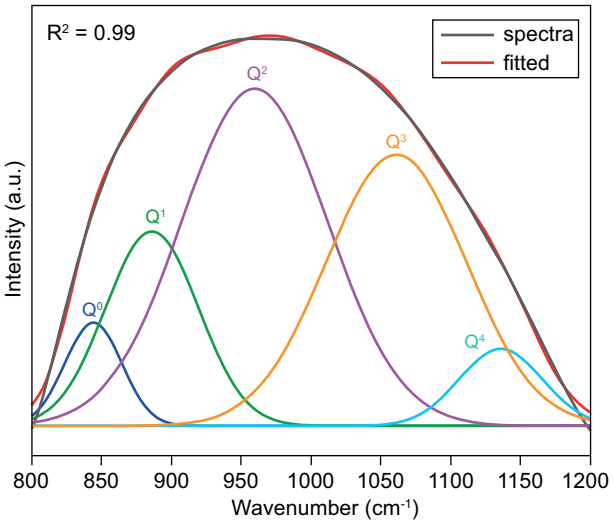

e) A5

Figure 5. Deconvoluted infrared spectra (800 to 1200 cm^{-1}) of glass with different Al_2O_3/SiO_2.

decomposed into stretching vibration of silicon-oxygen tetrahedron with different degree of polymerization by Gaussian function, whose symbol is Q^n, where n is the number of bridging oxygen (O_b) in the silicon-oxygen tetrahedron ($n = 0, 1, 2, 3, 4, 5$) [19, 28]. Figure 5 was the Gaussian deconvolution diagram of the infrared vibration absorption peak at the range of 800 to 1200 cm^{-1} of the glass, and Table 5 was the peak position and relative area of Q^n. The vibration absorption peaks at 800 to 1200 cm^{-1} were all decomposed into 5 vibration absorption peaks corresponding to Q^0, Q^1, Q^2, Q^3 and Q^4 respectively.

Figure 6a was the variation distribution chart of peak position of Q^n, which indicated that the peak position of Q^n was firstly shifted to direction of the low wavenumbers and then to the high wavenumbers, among which the peak position of Q^n reached the lowest when

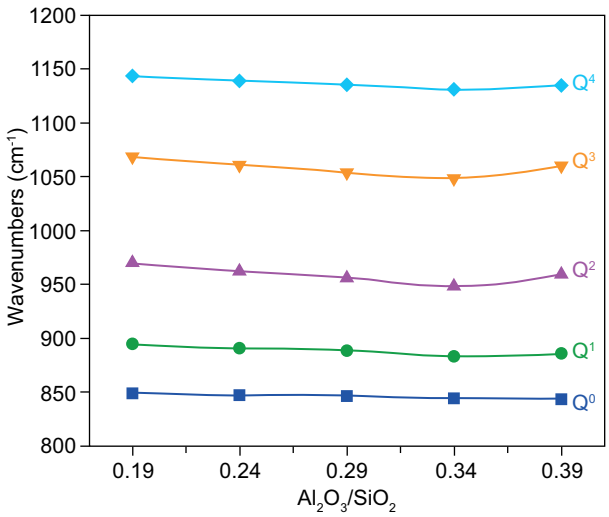

a) Peak position of Q^n

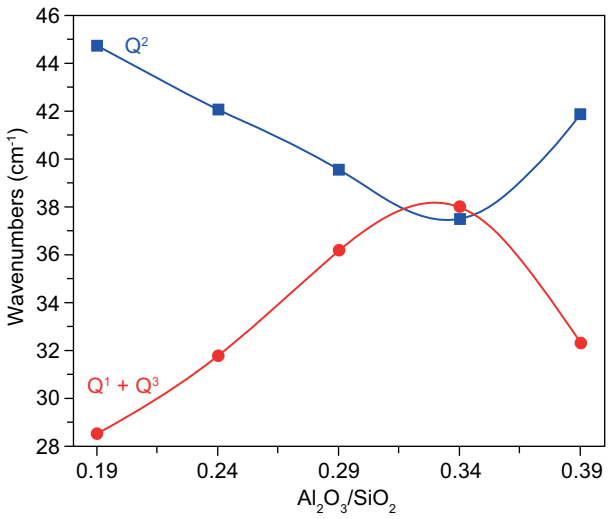

b) Area % of Q^2 and Q^1+Q^3

Figure 6. Peak position and Area % of Q^n in glass with different Al_2O_3/SiO_2.

the Al_2O_3/SiO_2 was 0.34 (A4). The vibration absorption peak of Q^n is closely related to the glass network [29]. The curve in fig. 6 (a) illustrated that the glass network structure tended to be loose with the increase of Al_2O_3/SiO_2 from 0.19 to 0.34; subsequently, the glass network structure tended to be close with the Al_2O_3/SiO_2 continued to increase from 0.34 to 0.39 [29]. The relative area of Q^n is related to the content, as can be seen in Figure 6b, Q^2 first decreased and then increased, while (Q^1+Q^3) changed in the opposite way. We assumed that with the increase of Al_2O_3/SiO_2, Q^2 in the glass structure transformed to Q^1 and Q^3 gradually, and the content of Q^2 reached the minimum when the Al_2O_3/SiO_2 was 0.34. At this time, when the Al_2O_3/SiO_2 continued to increase, Q^1 and Q^3 transformed to Q^2.

Table 5. Wavenumbers and relative area of Qn in glass with different Al_2O_3/SiO_2.

		A1	A2	A3	A4	A5
Wavenumbers (cm^{-1})	Q^0	849.7	847.2	847.1	844.1	844.1
	Q^1	894.6	890.6	889.0	883.5	886.2
	Q^2	970.2	962.4	956.6	948.4	959.6
	Q^3	1069.5	1061.6	1054.5	1049.2	1060.9
	Q^4	1144.7	1140.1	1136.5	1132.2	1135.9
Relative area (%)	Q^0	5.258	5.354	4.764	4.749	5.020
	Q^1	17.795	16.585	15.086	13.812	15.380
	Q^2	44.750	42.069	39.558	37.505	41.847
	Q^3	28.539	31.783	36.174	37.999	32.304
	Q^4	3.658	4.209	4.417	5.935	5.449
	Q^1+Q^3	46.334	48.368	51.260	51.811	47.684

The infrared vibration absorption spectra of the glass-ceramics were showed in Figure 7. It indicated that the peak range of the glass-ceramics sample was roughly the same as that of the base glasses (Figure 4), which was still divided into three vibration absorption bands, however, there were some sharp absorption peaks which were not found in the infrared vibration absorption spectra of the base glass. This was mainly attributed to the generation of crystal phase, which made the originally covered absorption peaks appear [21, 23].

In the range of 400 to 600 cm^{-1}, the vibration absorption peak at 470 cm^{-1} was divided into two absorption peaks: 472 cm^{-1} and 424 cm^{-1}. The peak at 472 cm^{-1} was attributed to the bending vibration of Si–O–Si in the residual glass phase and diopside phase (a small amount of hyalophane), the peak at 424 cm^{-1} was attributed to the bending vibration of Si–O–Al bond in gehlenite [24, 30]. There were two vibration absorption peaks at 544 cm^{-1} and 579 cm^{-1}, which were not found in the base glass in Figure 4. This was due to the coupling effect between the bending vibration of O–Si–O in the crystal phase and the stretching vibration of Ca–O [24, 27]. In the range of 600 to 800 cm^{-1}, in addition to the vibration absorption peak near 714 cm^{-1} (base glasses also had the same vibration absorption peak), two new vibration absorption peaks appeared at 682 cm^{-1} and 630 cm^{-1}. The peak at 714 cm^{-1} and 682 cm^{-1} were attributed to the symmetric stretching vibration of Si–O–Si and the stretching vibration of Si–O–Al respectively; the peak at 630 cm^{-1} was related to the stretching vibration of Al–O in the aluminum-oxygen tetrahedron [22, 27, 30]. In the range of 800-1200 cm^{-1}, the vibration absorption peak near 1000 cm^{-1} split into 1028 cm^{-1}, 985 cm^{-1} and 939 cm^{-1} due to crystal phase precipitation, which were associated with the stretching vibration of Si–O in [SiO_4] [22, 26, 27].

^{27}Al NMR analysis

To further study the coordination of Al^{3+} in glass, the ^{27}Al MAS NMR spectra were used to investigate the glass structure, as shown in Figure 8, there was an obvious wide peak in the range of -25 ppm to 100 ppm.

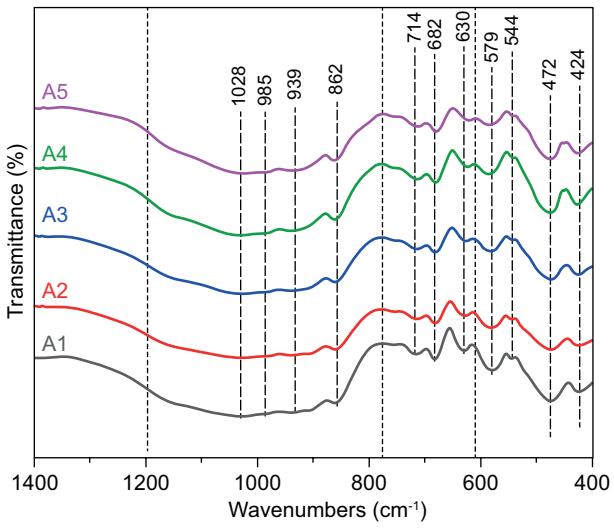

Figure 7. FTIR of glass-ceramics with different Al_2O_3/SiO_2.

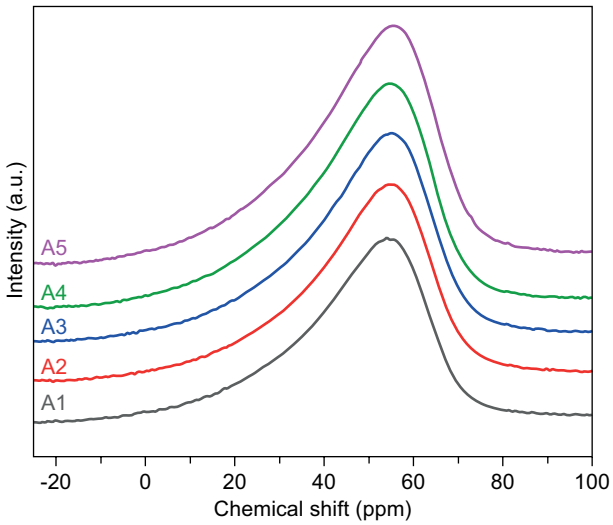

Figure 8. ^{27}Al NMR spectra of the glass with different Al_2O_3/SiO_2.

In aluminosilicate system, Al^{3+} has three coordination modes: [AlO_4], [AlO_5], [AlO_6] [31, 32]. Therefore, ^{27}Al NMR spectra were deconvoluted by Gaussian function, and the results were shown in Figure 9 and Figure 10.

The area % of [AlO_n] (n = 4, 5, 6) was related to its content [10]. In Figure 10, the area % of [AlO_6] decreased first, then increased and then decreased, reaching the maximum at A4 (Al_2O_3/SiO_2 was 0.34), on the contrary, the area % of [AlO_5] and [AlO_4] increased first, then decreased and then increased, reaching the minimum at A4. The area % of [AlO_6] in A1 glass was

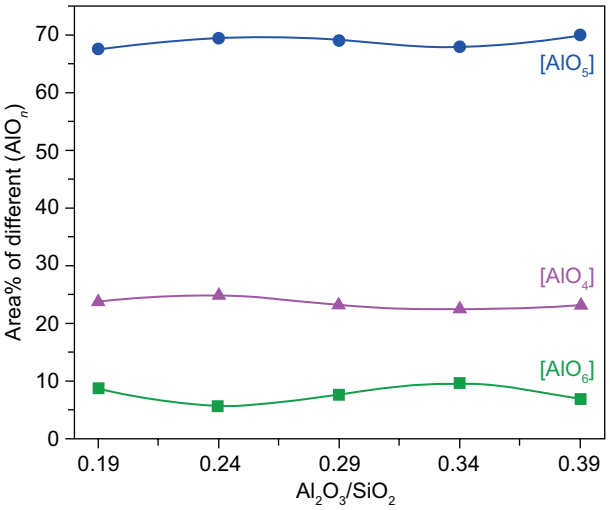

Figure 10. Area % of different [AlOn] in patent glass with different Al_2O_3/SiO_2; n = 4, 5, 6.

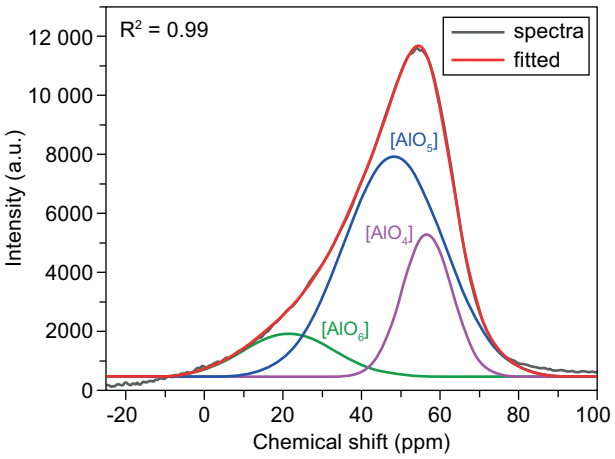

a) A1

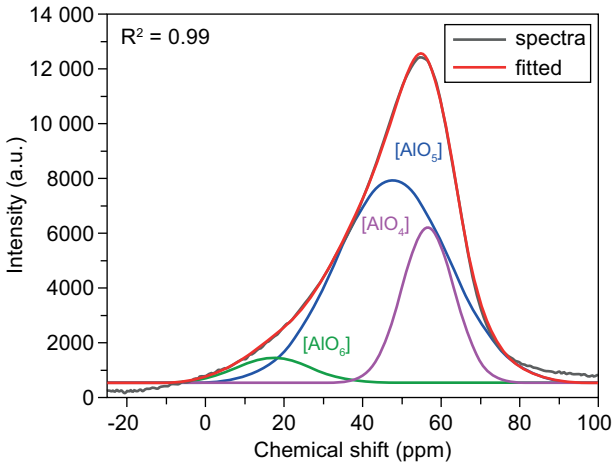

b) A2

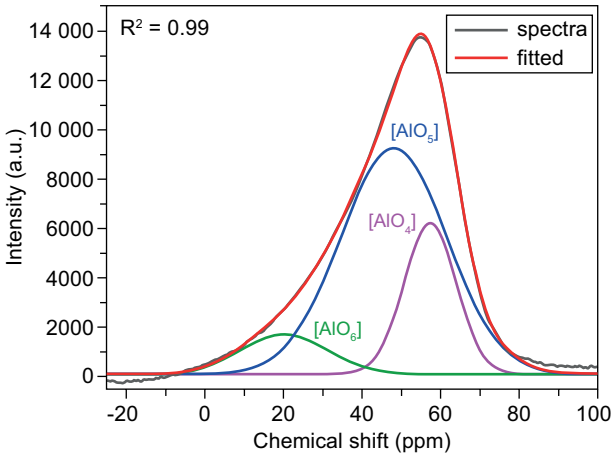

d) A4

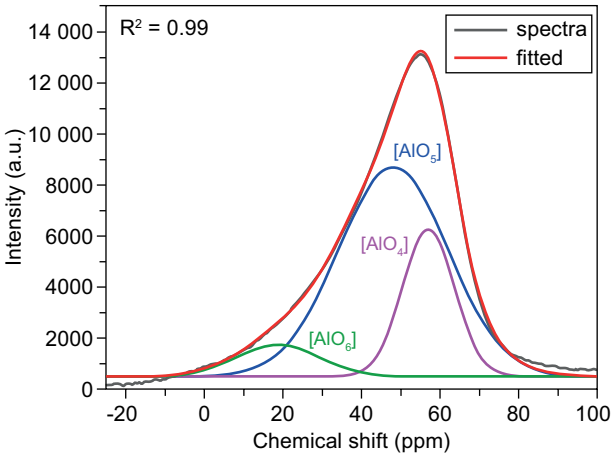

c) A3

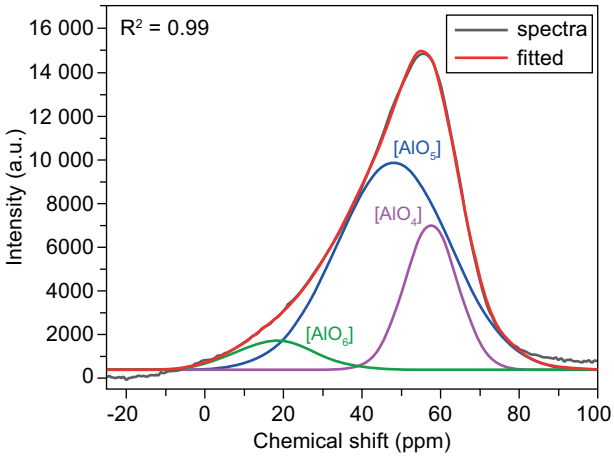

e) A5

Figure 9. Deconvolution of the ^{27}Al NMR spectra for glass with different Al_2O_3/SiO_2.

relatively large, while area % of [AlO_5] and [AlO_4] were relatively small, which may be related to the small Al_2O_3/SiO_2 in A1. The high SiO_2 content in the glass made the glass network densified, at the same time, the low Al_2O_3 content made it difficult for Al^{3+} to replace Si^{4+} in glass network.

Physical and mechanical properties analysis

The physical and mechanical properties of glass-ceramics with different Al_2O_3/SiO_2 were showed in Figure 11a-c were the bulk density, the bending strength and the microhardness respectively.

The results of Figure 11 showed that the volume density of the glass-ceramics was between 2.735 to 2.770 g·cm^{-3}, the bending strength was between 95.8 to 120.5 MPa and the microhardness was between 540.36 to 610.21 Hv. Meanwhile, with the increase of Al_2O_3/SiO_2, the bulk density, bending strength and microhardness of glass-ceramics all decreased first (reached the minimum in A4, the Al_2O_3/SiO_2 was 0.34) and then increased. The physical and mechanical properties of glass-ceramics are closely connected to the crystal phase, the glass phase and the combination among them [33, 34]. With the increase of Al_2O_3/SiO_2, the precipitation of gehlenite in the glass-ceramics increased, while the precipitation of diopside and hyalophane decreased, however, the density of gehlenite was lower than that of diopside and hyalophane, the bulk density of glass-ceramics decreased. When Al_2O_3/SiO_2 continued to increase to 0.39, the bulk density of glass-ceramics increased, which may be related to the growth of grain. The flexural strength and microhardness of the glass-ceramics reached the minimum at A4, the strength of Al–O bond in the glass structure was weaker than that of Si–O bond, and [AlO_6] was not conducive to the improvement of the flexural strength and microhardness compared with [AlO_4] [10]. Therefore, we assumed that the lower flexural strength and microhardness of A4 glass-ceramics were related to the lower bonding strength of [AlO_6] and Al–O bond.

CONCLUSION

The effects of Al_2O_3/SiO_2 on the structure and properties of Ca–Mg–Al–Si glass-ceramics were studied. When Al_2O_3/SiO_2 increased from 0.19 to 0.34, Q^2 transformed to Q^1 and Q^3 gradually. When Al_2O_3/SiO_2 continued to increase from 0.34 to 0.39, Q^1 and Q^3 decreased while Q^2 increased. With the increase of Al_2O_3/SiO_2, the degree of network polymerization of glass decreased first and then increased, and reached the minimum when Al_2O_3/SiO_2 was 0.34. The bulk density, bending strength and microhardness of glass-ceramics also had the same variation rule. At the same time, the increase of Al_2O_3/SiO_2 promoted the precipitation of

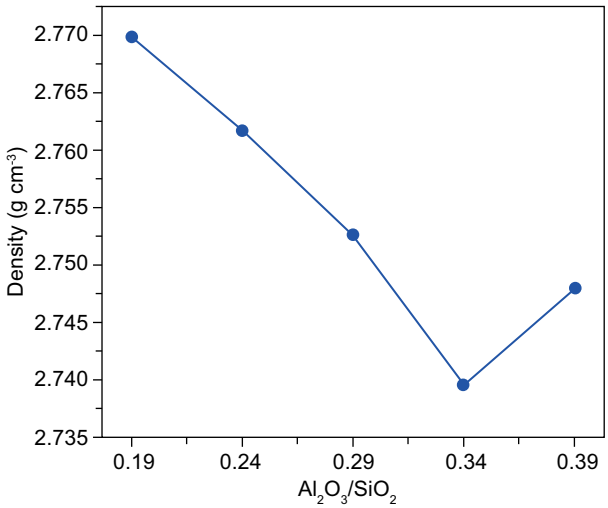

a) Bulk density of glass-ceramics

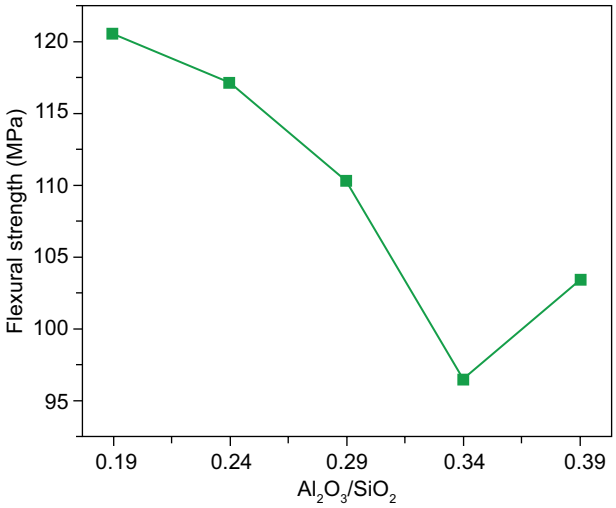

b) Bending strength of glass-ceramics

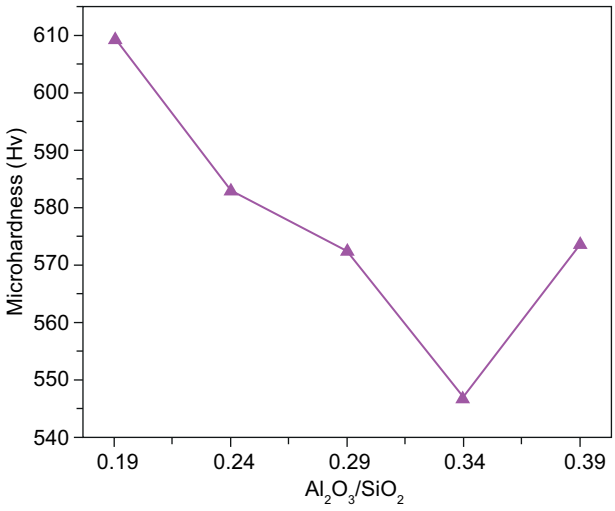

c) Microhardness of glass-ceramics

Figure 11. Physical and mechanical properties of glass-ceramics with different Al_2O_3/SiO_2.

gehlenite while hindered the precipitation of diopside and hyalophane in glass-ceramics. Glass-ceramics exhibited the highest bulk density, bending strength and microhardness when Al_2O_3/SiO_2 was 0.19, which were 2.770 g·cm^{-3}, 120.5 MPa and 610.21 Hv respectively.

Acknowledgement

We acknowledge Dr. Yumei Li (Center for Material research and analysis, Wuhan University of Technology, China) for the FESEM analyses.

REFERENCES

1. Jia R., Deng L., Yun F., Li H., Zhang X., Jia X. (2019): Effects of SiO_2/CaO ratio on viscosity, structure, and mechanical properties of blast furnace slag glass ceramics. *Materials Chemistry and Physics*, *233*, 155-162. doi: 10.1016/j.matchemphys.2019.05.065
2. He T., Li Z., Zhao S., Zhao X., Qu X. (2021): Study on the particle morphology, powder characteristics and hydration activity of blast furnace slag prepared by different grinding methods. *Construction and Building Materials*, *270*, 121-445. doi: 10.1016/j.conbuildmat.2020.121445
3. Oge M., Ozkan D., Celik M. B., Gok M. S., Karaoglanli A. C. (2019): An overview of utilization of blast furnace and steelmaking slag in various applications. *Materials Today: Proceedings*, *11*, 516-525. doi: 10.1016/j.matpr.2019.01.023
4. Deng B., Luo J., Harris J. T., Smith C. M., McKenzie M. E. (2019): Molecular dynamics simulations on fracture toughness of Al_2O_3–SiO_2 glass-ceramics. *Scripta Materialia*, *162*, 277-280. doi: 10.1016/j.scriptamat.2018.11.034
5. Dechandt I. C. J., Soares P., Pascual M. J., Serbena F. C. (2020): Sinterability and mechanical properties of glass-ceramics in the system SiO_2–Al_2O_3–MgO/ZnO. *Journal of the European Ceramic Society*, *40*(15), 6002-6013. doi: 10.1016/j.jeurceramsoc.2020.07.032
6. Diallo B., Allix M., Véron E., Sarou-Kanian V., Bardez-Giboire I., Montouillout V., Pellerin, N. (2019): Deconvolution method of 29Si MAS NMR spectra applied to homogeneous and phase separated lanthanum aluminosilicate glasses. *Journal of Non-Crystalline Solids*, *503*, 352-365. doi: 10.1016/j.jnoncrysol.2018.10.026
7. Novikov A. N., Neuville D. R., Hennet L., Gueguen Y., Thiaudière D., Charpentier T., Florian P. (2017): Al and Sr environment in tectosilicate glasses and melts: viscosity, Raman and NMR investigation. *Chemical Geology*, *461*, 115-127. doi: 10.1016/j.chemgeo.2016.11.023
8. Kwinda T. I., Koppka S., Sander S. A., Kohns R., Enke D. (2020): Effect of Al_2O_3 on phase separation and microstructure of R_2O–B_2O_3–Al_2O_3–SiO_2 glass system (R = Li, Na). *Journal of Non-Crystalline Solids*, *531*, 119849. doi: 10.1016/j.jnoncrysol.2019.119849
9. Zhang W., He F., Xiao Y., Xie M., Xie J., Sun R., et al. (2019): Effects of Al/Na and heat treatment on the structure and properties of glass ceramics from molten blast furnace slag. *Ceramics International*, *45*(11), 13692-13700. doi: 10.1016/j.ceramint.2019.04.064
10. Zhang W., He F., Xiao Y., Xie M., Xie J., Li F., et al. (2020): Structure, crystallization mechanism, and properties of glass ceramics from molten blast furnace slag with different B_2O_3/Al_2O_3. *Materials Chemistry and Physics*, *243*, 122-664. doi: 10.1016/j.matchemphys.2020.122664
11. Chen L., Ge X., Long Y., Zhou M., Wang H., Chen X. (2020): Crystallization and properties of high calcium glass-ceramics synthesized from ferromanganese slag. *Journal of Non-Crystalline Solids*, *532*, 119864. doi: 10.1016/j.jnoncrysol.2019.119864
12. Cheng J., Xiao Z., Yang K., Wu H. (2013): Viscosity, fragility and structure of Na_2O–CaO–Al_2O_3–SiO_2 glasses of increasing Al/Si ratio. *Ceramics International*, *39*(4), 4055-4062. doi: 10.1016/j.ceramint.2012.10.258
13. Partyka J., Leśniak M. (2016): Raman and infrared spectroscopy study on structure and microstructure of glass-ceramic materials from SiO_2–Al_2O_3–Na_2O–K_2O–CaO system modified by variable molar ratio of SiO_2/Al_2O_3. *Spectrochimica Acta Part A: Molecular and Biomolecular Spectroscopy*, *152*, 82-91. doi: 10.1016/j.saa.2015.07.045
14. Zeng L., Sun H. J., Peng T. J., Zheng W. M. (2019): The sintering kinetics and properties of sintered glass-ceramics from coal fly ash of different particle size. *Results in Physics*, *15*, 102774. doi: 10.1016/j.rinp.2019.102774
15. Jiang C., Li K., Zhang J., Qin Q., Liu Z., Sun, M., et al. (2018): Effect of MgO/Al_2O_3 ratio on the structure and properties of blast furnace slags: A molecular dynamics simulation. *Journal of Non-Crystalline Solids*, *502*, 76-82. doi: 10.1016/j.jnoncrysol.2018.06.043
16. Karamanov A., Hamzawy E. M., Karamanova E., Jordanov N. B., Darwish H. (2020): Sintered glass-ceramics and foams by metallurgical slag with addition of CaF_2. *Ceramics International*, *46*(5), 6507-6516. doi: 10.1016/j.ceramint.2019.11.132
17. Li B., Li W., Zheng J. (2017): Effect of SiO_2 content on the sintering kinetics, microstructures and properties of BaO–Al_2O_3–B_2O_3–SiO_2 glass-ceramics for LTCC application. *Journal of Alloys and Compounds*, *725*, 1091-1097. doi: 10.1016/j.jallcom.2017.07.251
18. Zhang W., He F., Xie J., Liu X., Fang D., Yang H., Luo Z. (2018): Crystallization mechanism and properties of glass ceramics from modified molten blast furnace slag. *Journal of Non-Crystalline Solids*, *502*, 164-171. doi: 10.1016/j.jnoncrysol.2018.08.024
19. Deng L., Jia R., Yun F., Zhang X., Li H., Zhang M., et al. (2020): Influence of Cr_2O_3 on the viscosity and crystallization behavior of glass ceramics based on blast furnace slag. *Materials Chemistry and Physics*, *240*, 122-212. doi: 10.1016/j.matchemphys.2019.122212
20. Akatov A. A., Nikonov B. S., Omel'Yanenko B. I., Stefanovsky S. V., Marra J. C. (2009): Structure of borosilicate glassy materials with high concentrations of sodium, iron, and aluminum oxides. *Glass Physics and Chemistry*, *35*(3), 245-259. doi: 10.1134/S1087659609030031
21. Ma M., Ni W., Wang Y., Wang Z., Liu F. (2008): The effect of TiO_2 on phase separation and crystallization of glass-ceramics in CaO–MgO–Al_2O_3–SiO_2–Na_2O system. *Journal of Non-Crystalline Solids*, *354*(52-54), 5395-5401. doi: 10.1016/j.jnoncrysol.2008.09.019
22. Deng L., Yun F., Jia R., Li H., Jia X., Shi Y., Zhang X. (2020): Effect of SiO_2/MgO ratio on the crystallization behavior, structure, and properties of wollastonite-augite glass-ceramics derived from stainless steel slag. *Materials*

Chemistry and Physics, *239*, 122039. doi: 10.1016/j.matchemphys.2019.122039

23. Shi J., He F., Ye C., Hu L., Xie J., Yang H., Liu X. (2017): Preparation and characterization of $CaO–Al_2O_3–SiO_2$ glass-ceramics from molybdenum tailings. *Materials Chemistry and Physics*, *197*, 57-64. doi: 10.1016/j.matchemphys.2017.05.028
24. Luo W., Bao Z., Jiang W., Liu J., Feng G., Xu Y., et al. (2019): Effect of B_2O_3 on the crystallization, structure and properties of $MgO–Al_2O_3–SiO_2$ glass-ceramics. *Ceramics International*, *45*(18), 24750-24756. doi: 10.1016/j.ceramint.2019.08.215
25. Kim E. S., Yeo W. J. (2012): Thermal properties of $CaMgSi_2O_6$ glass-ceramics with Al_2O_3. *Ceramics International*, *38*, S547-S550. doi: 10.1016/j.ceramint.2011.05.074
26. Ghosh T. K., pradip Mukherjee D., Ghorai U. K., Das S. K. (2019): Synthesis and crystallisation kinetics study of nano-Al_2O_3 containing bio-active glass-ceramics. *Materials Today: Proceedings*, *11*, 794-803. doi: 10.1016/j.matpr.2019.03.045
27. Montoya-Quesada E., Villaquirán-Caicedo M. A., de Gutiérrez R. M., Muñoz-Saldaña J. (2020): Effect of ZnO content on the physical, mechanical and chemical properties of glass-ceramics in the $CaO–SiO_2–Al_2O_3$ system. *Ceramics International*, *46*(4), 4322-4328. doi: 10.1016/j.ceramint.2019.10.154
28. Zhao M., Cao J., Wang Z., Li G. (2019): Insight into the dual effect of Fe_2O_3 addition on the crystallization of $CaO–MgO–Al_2O_3–SiO_2$ glass-ceramics. *Journal of Non-Crystalline Solids*, *513*, 144-151. doi: 10.1016/j.jnoncrysol.2019.03.021
29. Chen, M., He, F., Shi, J., Xie, J., Yang, H., & Wan, P. (2019): Low Li_2O content study in $Li_2O–Al_2O_3–SiO_2$ glass-ceramics. *Journal of the European Ceramic Society*, *39*(15), 4988-4995. doi: 10.1016/j.jeurceramsoc.2019.07.032
30. Pei F., Guo H., Li P., Yan B., Li J., Yang P., Zhu G. (2018): Influence of low magnesia content on the $CaO–Al_2O_3–SiO_2$ glass-ceramics: its crystallization behaviour, microstructure and physical properties. *Ceramics International*, *44*(16), 20132-20139. doi: 10.1016/j.ceramint.2018.07.306
31. Wilson P. T., Chahal S., Kumar M. M., Ramesh K. (2019): ^{27}Al MAS NMR investigations on $Al_{23}Te_{77}$ glass: Observation of 5-coordinated Al and its influence on electrical switching. *Solid State Communications*, *293*, 53-57. doi: 10.1016/j.ssc.2019.02.007
32. Kusumoto H., Hill R. G., Karpukhina, N., Law R. V. (2019): Magnesium substitution in calcium and strontium fluorophospho-aluminosilicate glasses by multinuclear ^{19}F, ^{31}P, ^{27}Al, and ^{29}Si MAS-NMR spectroscopy. *Journal of Non-Crystalline Solids: X*, *1*, 100008. doi: 10.1016/j.nocx.2019.100008
33. Inage K., AkatsukaK., Iwasaki K., Nakanishi T., Maeda K., Yasumori A. (2020): Effect of crystallinity and microstructure on mechanical properties of $CaO–Al_2O_3–SiO_2$ glass toughened by precipitation of hexagonal $CaAl_2Si_2O_8$ crystals. *Journal of Non-Crystalline Solids*, *534*, 119948. doi: 10.1016/j.jnoncrysol.2020.119948
34. Gui H., Li C., Lin C., Zhang Q., Luo Z., Han L., et al. (2019): Glass forming, crystallization, and physical properties of $MgO–Al_2O_3–SiO_2–B_2O_3$ glass-ceramics modified by ZnO replacing MgO. *Journal of the European Ceramic Society*, *39*(4), 1397-1410. doi: 10.1016/j.jeurceramsoc.2018.10.002